Analysis of Physical Processes in ICF Target Chambers: Application to the Laboratory Microfusion Facility

J.J. MacFarlane, R.R. Peterson, G.A. Moses

October 1988

UWFDM-776

Presented at the 8th Topical Meeting on the Technology of Fusion Energy, 9–13 October 1988, Salt Lake City UT; Fusion Tech. 15, 557.

FUSION TECHNOLOGY INSTITUTE

UNIVERSITY OF WISCONSIN

MADISON WISCONSIN

Analysis of Physical Processes in ICF Target Chambers: Application to the Laboratory Microfusion Facility

J.J. MacFarlane, R.R. Peterson, G.A. Moses

Fusion Technology Institute
University of Wisconsin
1500 Engineering Drive
Madison, WI 53706

http://fti.neep.wisc.edu

October 1988

UWFDM-776

Presented at the 8th Topical Meeting on the Technology of Fusion Energy, 9–13 October 1988, Salt Lake City UT; Fusion Tech. 15, 557.

ANALYSIS OF PHYSICAL PROCESSES IN ICF TARGET CHAMBERS: APPLICATION TO THE LABORATORY MICROFUSION FACILITY

J. J. MacFarlane, R. R. Peterson, and G. A. Moses
Fusion Technology Institute, Dept. of Nuclear Engineering and Engineering Physics
University of Wisconsin, 1500 Johnson Drive, Madison, WI 53706-1687
(608) 263-8485

ABSTRACT

When a high-gain inertial fusion target explodes, roughly one third of the energy will be released in the form of x-rays and energetic ions, which can damage the wall of the chamber. One method of protecting the wall is to place a gas in the chamber cavity. We use a 1-D Lagrangian radiation-hydrodynamics code (CONRAD) to study the target energy deposition in this cavity gas and first surface material, the growth of and radiative emission from the microfireball, the expansion of the shock front, the vaporization and hydromotion of the first surface material, and the recondensation of that material back onto the wall. We describe recent improvements to CONRAD, and present results for two target chamber designs currently being considered by Lawrence Livermore National Laboratory for the Laboratory Microfusion Facility.

INTRODUCTION

The response of the cavity gas and first surface (wall) material to a target explosion is a prime concern in designing ICF target chambers. Structural damage to the wall could result from shock-produced impulses if the chamber radius is too small. In addition, significant vaporization of wall material can lead to several problems: a large recoil impulse and high instantaneous pressures at the cavity/wall interface, an excessive erosion rate, and in the case of reactors, the condensation times of vaporized material may exceed the desired repetition rate.

We expect inertial confinement fusion (ICF) driver beams to ignite fusion targets and release up to 1000 MJ of energy in the form of neutrons, x-rays, and energetic ions. Approximately 25% to 40% of the target yield will be in x-rays and debris ions. The protective cavity gas density in the target chamber, and therefore the ion and x-ray deposition characteristics, will be determined by the beam transport requirements of the driver (laser, light ion, or heavy ion). When the background gas density is low ($<< 10^{16}$ cm^{-3}), most of the x-ray energy is deposited directly at the wall, producing significant ablation (vaporization) of the wall material. When a substantial background gas is present, the x-ray and ion energy is absorbed by the gas, creating a high temperature plasma which drives a strong shock wave. The radiative flux and the strength of the shock at the chamber wall are strongly influenced by the radiative properties of the plasma.

Below, we will describe the general features of the computer code we use to study the physical processes that will occur in ICF target chambers. In particular, we will emphasize recent improvements to CONRAD in two areas: (1) the plasma equation of state and radiative properties, and (2) the vaporization/condensation model. We will also describe the results of numerical simulations relevant to the LLNL Laboratory Microfusion Facility (LMF).[1] We have considered 2 chamber designs for the LMF. In each case, the chamber radius is 8 meters, and the first surface is composed of graphite. The single difference between the 2 designs is that in one case the target explodes in a hard vacuum, while in the other the background gas density is 3 x 10^{16} cm^{-3} of argon. In each case, the total energy released by the target is 1000 MJ, of which 200 MJ is in x-rays and 200 MJ is in debris ions.

PHYSICAL MODELS

The computer code used to study target chamber phenomena, CONRAD,[2] is a 1-D Lagrangian radiation-hydrodynamics code. A multigroup flux-limited diffusion model is used to transport radiation. Target x-rays are deposited in the background gas and first surface using a time-dependent attenuation model.[3] Energy from the target debris ions is deposited with a time-dependent stopping power model[4] which includes high-temperature effects of the stopping medium. In addition, CONRAD simulates the vaporization,

hydrodynamic motion, and condensation of the first surface material.

A detailed description of the physics models in CONRAD are provided elsewhere.[2] Below, we describe recent improvements to the code.

A. Plasma Properties

Plasma temperatures and densities in the protective gas in ICF target chambers after a high-gain pellet explosion are typically ~ 1-100 eV and 10^{12} - 10^{19} cm^{-3}, respectively, depending on the initial gas density. At relatively low temperatures and high densities, 3-body (collisional) reactions dominate all atomic processes -- ionization, recombination, excitation, and deexcitation. In this case, the plasma is in local thermodynamic equilibrium (LTE), and the ionization and excitation populations can be calculated using the usual Saha equation and Boltzmann statistics.[5] However, at relatively high temperatures and low densities, 2-body (radiative) recombination and deexcitation rates exceed the collisional rates, and the LTE approximation is invalid. Thus, both 2-body and 3-body processes must be fully considered in calculating the equations of state and radiative properties of ICF target chamber plasmas.

We have developed a computer code (IONMIX) that computes equations of state and multigroup opacities for LTE and non-LTE plasmas.[6] The ionization populations are determined by balancing the collisional ionization rate with the sum of the collisional, radiative, and dielectronic recombination rates. Similarly, the excitation populations for each ion are calculated by balancing the collisional excitation rate with the collisional plus radiative deexcitation rates. One can assess whether a plasma is in LTE by examining the ratio of the collisional recombination rate to the sum of the radiative and dielectronic recombination rates. This ratio is shown in Figure 1 for nitrogen as a function of density at 3 different temperatures. For each temperature, the recombination rates shown correspond to the most abundant ionization state: N^{1+} -> N^{0+} at 1 eV, N^{4+} -> N^{3+} at 10 eV, and N^{6+} -> N^{5+} at 100 eV. The shaded area represents the regime of temperatures and densities relevant to target chamber plasmas. When the collisional rate is much greater than the radiative and dielectronic recombination rates, the plasma is in LTE. Figure 1 shows that target chamber plasmas with temperatures $\gtrsim$ 10 eV are not in LTE. However, it is also clear that collisional recombination effects cannot be neglected for plasmas with temperatures less than 10 eV and densities $\gtrsim$ 10^{18} cm^{-3}.

At high temperatures, non-LTE (2-body) processes produce a depopulation of upper ionization and excitation states relative to

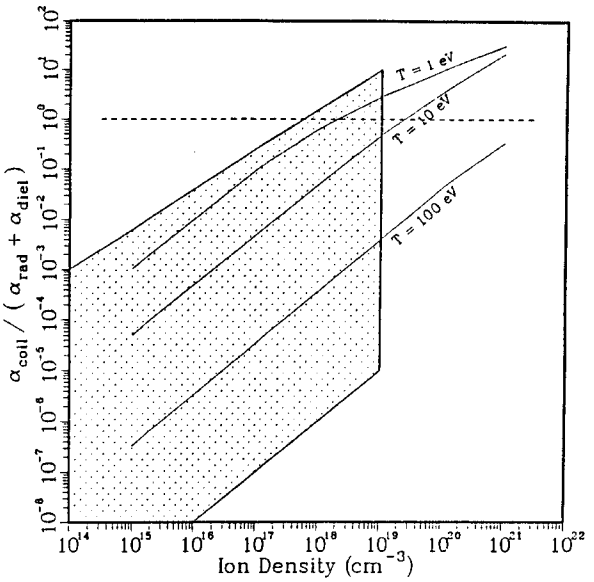

Fig. 1. Ratio of collisional recombination rate to sum of radiative and dielectronic recombination rates for nitrogen as a function of density at temperatures of 1, 10, and 100 eV. Shaded region represents regime of densities and temperatures relevant to ICF target chambers.

LTE, and thus a decrease in the mean charge state and specific energy. In addition, the plasma emission rate can be significantly reduced for the same reason. This can be seen by examining the ratio of the Planck mean opacities for emission and absorption:

$$\sigma_P^E \; / \; \sigma_P^A \; = \; \frac{\int d\nu \; \eta_\nu}{\int d\nu \; \kappa_\nu \; B_\nu}$$

where ν is the photon frequency, η_ν is the emissivity, κ_ν is the absorption coefficient, and B_ν is the Planck function. This ratio is plotted in Figure 2 for neon as a function of density at temperatures of 3, 30, and 300 eV. In LTE, the Planck-Kirchoff relation, $\eta_\nu = \kappa_\nu B_\nu$, is valid, and $\sigma_P^E = \sigma_P^A$. At low densities and high temperatures, non-LTE effects reduce the plasma emission rate by several orders of magnitude. The influence of non-LTE processes on ICF target chamber calculations has been described in more detail elsewhere.[7]

B. Vaporization/Condensation Model

Vaporization of the first surface in ICF target chambers effectively occurs in two phases. During the first phase, hard x-rays from the target travel at the speed of light to the wall and, because of their long mean free

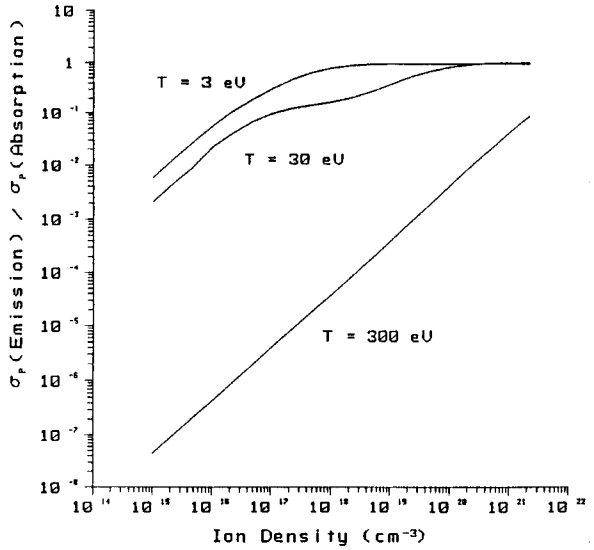

Fig. 2. Ratio of Planck mean absorption rate to emission rate for neon versus density at temperatures of 3, 30, and 300 eV.

paths, deposit their energy "volumetrically" in the first surface material. During the second phase, thermal radiation -- i.e., energy absorbed by the background gas and reemitted by the microfireball -- deposits its energy near the vapor/first surface interface. CONRAD models both effects, using a "volumetric" vaporization model for the hard target x-rays and a "surface" vaporization model at later times.

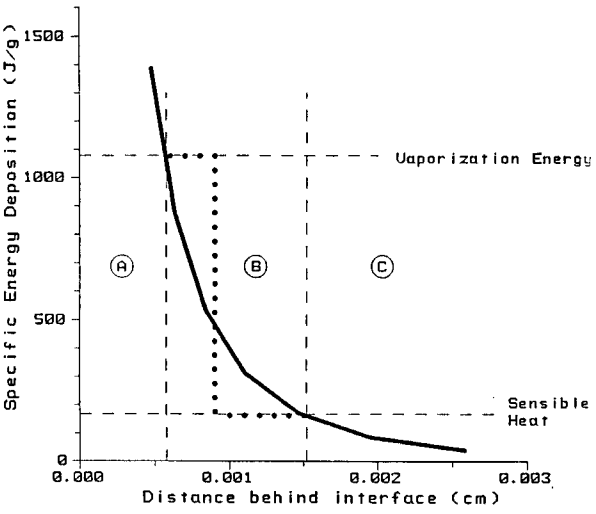

Fig. 3. Typical energy deposition profile in a first surface material.

Hard x-rays are deposited in the first surface material over a depth of ~ 10 μm. A typical energy deposition profile is illustrated in Figure 3, where the specific energy of the first surface material just after the target x-ray energy is deposited is plotted as a function of distance behind the vapor/first surface interface. In CONRAD, the surface material is divided into 3 regions. In region A, the energy density is higher than the vaporization energy density. All material in this region becomes superheated vapor. In region C, the energy density remains lower than the "sensible" energy density (i.e., the vaporization energy minus the heat of vaporization). None of this material is vaporized during the volumetric vaporization phase. In region B, the energy density lies between the vaporization and sensible energies, and the temperature throughout the region is equal to the vaporization temperature. To estimate the amount of material vaporized from region B, CONRAD redistributes the energy within this region so that all material is either at the vaporization energy or at the sensible energy, while maintaining energy conservation. The redistributed energy is represented by the dotted line in Figure 3.

When material is vaporized, the pressure of the vapor near the interface is very high because of the high particle density. This causes material to be rapidly accelerated away from the interface, and provides a "recoil" impulse to the wall. If either the instantaneous pressure or impulse are excessively large, the wall may sustain structural damage.

After the volumetric deposition phase, radiant energy transported to the condensed region will effectively be deposited at the surface of the interface because of the shorter photon mean free paths. The vaporization and condensation rates are then calculated using a kinetic theory approach described by Labuntsov and Kryukov.[8] The mass vaporization rate per unit area is:

$$(dm/dt)_v = \frac{2}{3}\left(\frac{\mu}{RT_v}\right)^{1/2} P_{sat}$$

where T_v is the vapor temperature, P_{sat} is the saturation vapor pressure, μ is the mean atomic weight, and R is the gas constant. The mass condensation rate per unit area is:

$$(dm/dt)_c = \frac{2}{3}\left(\frac{\mu}{RT_v}\right)^{1/2} P_v f_s f_{nc}$$

where P_v is the vapor pressure, f_s is the sticking coefficient, which represents the fraction of vapor atoms striking the wall that attach to it, and f_{nc} is a parameter which accounts for the presence of noncondensable gases.

In our simulations, Lagrangian cells undergo hydrodynamic motion only after the entire cell has been vaporized. No mixing occurs between cells. Energy is transported away from the vapor/first surface interface to the back of the condensed region by thermal conduction.

LMF NUMERICAL SIMULATIONS

We have used CONRAD to simulate the physical conditions for 2 target chamber designs currently being considered for the LLNL Laboratory Microfusion Facility (LMF). The design parameters are listed in Table 1. The two cases are identical except for the initial cavity gas conditions. In Case 1, the target explodes in a hard vacuum, while in Case 2 an initial background gas of 1 torr of argon surrounds the target. In each problem, the chamber wall has a radius of 8 meters and is lined with graphite.

Table 1. Cavity Parameters for LMF Simulations

	Case 1	Case 2
Total Target Yield (MJ)	1000	1000
X-ray Energy (MJ)	200	200
Debris Ion Energy (MJ)	200	200
Target Chamber Radius (m)	8	8
First Wall Material	graphite	graphite
Gas Species	carbon	argon
Initial Gas Density (cm^{-3})	3.5×10^{11}	3.5×10^{16}

We have analyzed the response of the cavity gas and graphite wall to 1000 MJ target explosions. We assume the target energy is partitioned into 20% x-rays, 20% debris ions, and 60% neutrons. Neutrons have long mean free paths and deposit essentially all of their energy beyond the first wall, and hence are not considered in the calculations. The target x-ray spectrum is shown in Figure 4. It basically consists of a 300 eV blackbody spectrum superimposed on a 15 keV blackbody spectrum. This x-ray spectrum was calculated for a target with a modest amount of high-Z material in its outer layers.[9] We have taken the target debris to be 500 keV Pb ions.

Results of the two calculations are summarized in Table 2 and Figures 5 through 8. Figure 5 shows the radiative flux at the wall for both cases as a function of time after the target explosion. When a 1 torr argon gas surrounds the target, approximately 86% of target x-ray energy is absorbed by the argon. This energy is in turn reradiated to the chamber wall over a period of roughly 100 μs. During this period, the radiant heat flux is ~ 10^6 W/cm^2 (dashed curve). When the target explodes in a hard vacuum, the target x-ray energy is deposited directly in the wall, vaporizing just over 2 kg of graphite. In this case, the radiative heat flux (neglecting the target x-rays) remains

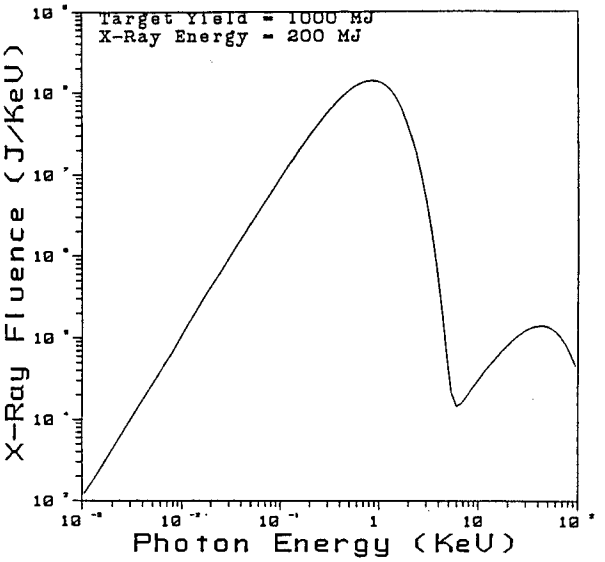

Fig. 4. Target x-ray spectrum.

relatively low until the debris ions are stopped in the carbon vapor at ~ 10 μs. As the vapor is heated, it radiates to the wall, producing a peak radiative flux of ~ 10^7 W/cm^2.

Table 2. Results from LMF Simulations

	Case 1	Case 2
Target x-ray energy deposited at wall (MJ)	200	28
Debris ion energy deposited at wall (MJ)	0	0
Maximum mass vaporized from wall (kg)	2.2	0.6
Maximum radiant heat flux on wall (MW/cm^2)	13	3.9
Total impulse on wall (Pa-s)	16	32

The amount of graphite vaporized is plotted as a function of time in Figure 6. When no background gas is present to absorb the x-rays, roughly 1 μm (or 2 kg) is immediately ablated from the wall. During this time, the instantaneous pressure at the cavity/wall interface becomes extremely high (~ 10 GPa) due to the high energy and particle densities. Similar pressures can also be reached when a background gas is present if the radiative flux at the wall is very large. Because these pressures can exceed the yield stress of the wall material, a

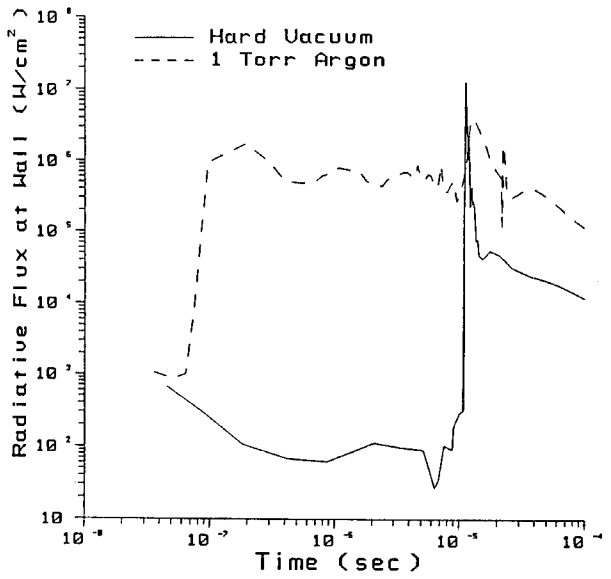

Fig. 5. Radiative heat flux at the wall versus time.

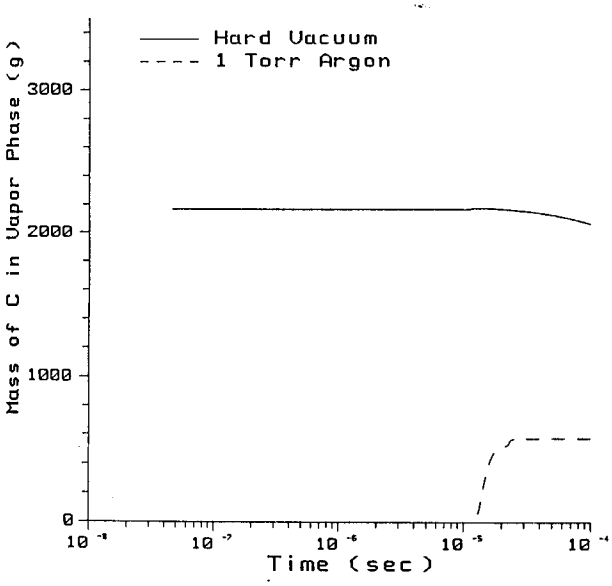

Fig. 6. Mass of carbon in the vapor phase versus time.

protective layer must be used to attenuate the resulting shocks.

Although the radiant heat flux at the wall in Case 1 becomes rather high just after the debris ions are stopped in the carbon vapor, little additional vaporization occurs. The reason for this can be seen in Figure 7, where the temperature at the inner surface of the

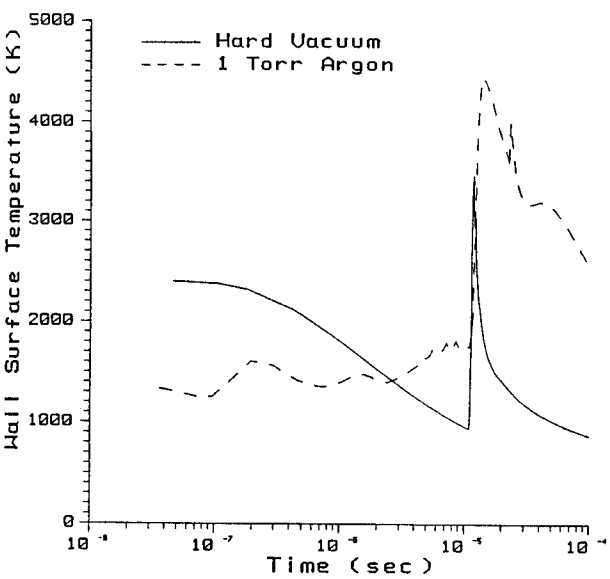

Fig. 7. Graphite wall surface temperature versus time.

graphite wall is plotted as a function of time. For the hard vacuum case (solid curve), the temperature drops to ~ 1000 K by 10 μs due to thermal conduction in the wall. When the heat flux increases due to the debris ion stopping, the wall surface temperature rises to roughly 3400 K before conduction again reduces the temperature at the surface. This temperature, however, is not high enough to produce significant additional vaporization.

When a 1 torr argon background gas is present, no vaporization occurs due to the target x-rays, but the wall surface is heated to about 1200 K. In this case, the debris ions are stopped in the argon within ~ 2 μs, increasing the total energy of the argon gas to about 360 MJ. Roughly 150 MJ of this energy is radiated to the wall in the period between 10 and 20 μs, vaporizing 0.6 kg (dashed line). Thus, the argon is seen to reduce the amount of graphite vaporized from the wall.

The motion of the argon gas and carbon vapor is shown in Figure 8 for Case 2, where the position of the Lagrangian zone boundaries is plotted as a function of time. The expanding target generated blast wave and the inward moving carbon vaporization front are clearly visible. At roughly 0.6 ms, the two fronts collide at about 4-5 meters from the chamber center. The strength of the outward moving shock is greatly attenuated by the carbon vapor. Because of this, the impulse at the wall due to the target generated shock is very small.

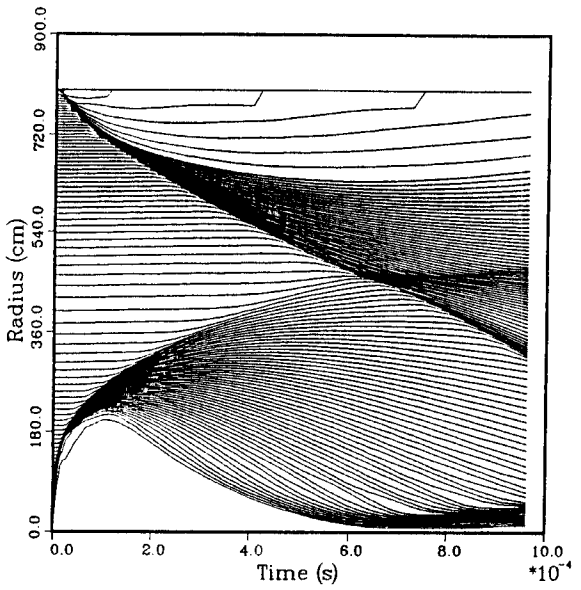

Fig. 8. Positions of Lagrangian zone boundaries versus time.

CONCLUSIONS

Protecting the wall from excessive ablation and thermal and mechanical stresses are critical considerations in designing ICF target chambers. We have shown that radiative processes are important in determining the equations of state and radiative properties of target chamber plasmas, and hence can affect predictions for the radiative heat flux and pressure impulse at the wall. We have also presented results from numerical simulations for the response of a target chamber wall to 1000 MJ pellet explosions for two designs currently being considered for the LLNL Laboratory Microfusion Facility. Our results indicate that when heat fluxes on the wall are high enough to cause vaporization, the resulting stresses are cause for serious concern.

ACKNOWLEDGEMENTS

Support for this work has been provided by Lawrence Livermore National Laboratory. Computing support has been provided by the National Science Foundation through the San Diego Supercomputer Center.

REFERENCES

1. W. J. HOGAN, "Target Chamber Design Issues for a High-Gain Inertial Fusion Test Facility," Bull. Amer. Phys. Soc., 32, 1788 (1987).

2. R. R. PETERSON, J. J. MacFARLANE, and G. A. MOSES, "CONRAD -- A Combined Hydrodynamics-Condensation/Vaporization Computer Code," UWFDM-670, University of Wisconsin Fusion Technology Institute Report (1988).

3. T. J. McCARVILLE, G. A. MOSES, and G. L. KULCINSKI, "A Model for Depositing Inertial Confinement Fusion X-rays and Pellet Debris into a Cavity Gas," UWFDM-406, University of Wisconsin Fusion Technology Institute Report (1981).

4. J. J. MacFARLANE, G. A. MOSES, and R. R. PETERSON, "Energy Deposition and Shock Wave Evolution from Laser-Generated Plasma Expansions," UWFDM-723, University of Wisconsin Fusion Technology Institute Report (1987), submitted to Phys. Fluids.

5. D. MIHALAS, Stellar Atmospheres, W. H. Freeman and Company, New York (1978).

6. J. J. MacFARLANE, "IONMIX -- A Code for Computing the Equation of State and Radiative Properties of LTE and Non-LTE Plasmas," UWFDM-750, University of Wisconsin Fusion Technology Institute Report (1987), submitted to Comput. Phys. Commun.

7. J. J. MacFARLANE, G. A. MOSES, and R. R. PETERSON, "Non-LTE Effects in Inertial Confinement Fusion Target Chambers," UWFDM-761, University of Wisconsin Fusion Technology Institute Report (1988), submitted to Nucl. Fusion.

8. D. A. LABUNTSOV and A. P. KRYUKOV, "Analysis of Intensive Evaporation and Condensation," Int. J. Heat Mass Transfer, 22, 989 (1979).

9. C. D. ORTH, "Improved Understanding of First-Wall Vaporization-Condensation in Inertial Confinement Fusion Reactors," Fusion Tech., 10, 1245 (1986).